Astron. Astrophys. 360, 1003–1010 (2000)

ASTRONOMY AND ASTROPHYSICS

A new orbital solution for the massive binary system HD 93403⋆

G. Rauw⋆⋆,†**, H. Sana, E. Gosset**⋆⋆⋆,†**, J.-M. Vreux, E. Jehin, and G. Parmentier**

Institut d'Astrophysique et de Géophysique, Université de Liège, 5, Avenue de Cointe, 4000 Liège, Belgium

Received 31 January 2000 / Accepted 15 June 2000

Abstract. We present a spectroscopic analysis of the early-type massive binary system HD 93403. Using high resolution optical spectra, we clearly separate the primary and secondary components. For the first time, we are able to provide an orbital solution for both stars. Our new orbital parameters show discrepancies with the previous solution published by Thackeray & Emerson (1969). We further discuss several spectral features of HD 93403. We finally derive qualitative constraints on the inclination of the system and we discuss its evolutionary status and the position of both components in the Hertzsprung-Russell diagram.

Key words: stars: binaries: spectroscopic – stars: early-type – stars: fundamental parameters – stars: individual: HD 93403

1. Introduction

HD 93403 is a relatively bright ($V = 7.3$) early-type star of the southern sky. Lying within the H II region NGC 3372 near η Car, it has long been known to be a single-lined spectroscopic binary (Feast et al. 1955). Walborn (1972) classified the spectrum of HD 93403 as O5 III:f. Based on the ratio of the equivalent widths of the He I λ 4471 and He II λ 4541 absorption lines, Conti & Frost (1977) reported HD 93403 as being an O5.5:f. Based on a tomographic study of a set of IUE spectra by Penny (1997), Thaller (1997) quoted spectral types O5 III + O7 III for HD 93403.

The only published orbital solution for HD 93403 we are aware of is 30 years old (Thackeray & Emerson 1969, TE hereafter). These authors determined an orbital period of 15.093 days, an eccentricity of 0.524 and a mass ratio close to 1.5. However, due to the rather limited quality of their data, TE were unable to disentangle the secondary spectrum, except on a few plates taken when the radial velocity separation between the two components was near maximum. Thackeray & Emerson guessed the spectral type of the fainter component to be O7.5, although they cautioned that this result was quite uncertain. These authors further mentioned photometric observations of HD 93403 that apparently failed to reveal eclipses.

HD 93403 was detected as a fairly bright X-ray source with the EINSTEIN satellite (Seward et al. 1979) and has been selected for observations with ESA's X-ray Multi Mirror (XMM) observatory. The analysis of these X-ray data, especially in terms of a colliding wind interaction (Pittard & Stevens 1997), requires an accurate knowledge of the orbital parameters of the system. As a first step, we derive therefore a new orbital solution for HD 93403. Using high resolution spectra obtained with the CES and FEROS instruments of the European Southern Observatory at La Silla and with the BME spectrograph at CTIO, we clearly separate the primary and secondary spectra, which means that HD 93403 should now be classified as an SB2 system.

This paper is organized as follows: the observations, data reduction and spectral features are discussed in Sect. 2; in Sect. 3, the radial velocities are used to set up a new orbital solution for both components of HD 93403. The fundamental parameters of the system are discussed in Sect. 4. Finally, our conclusions are presented in Sect. 5.

2. Observations and Data Reduction

2.1. Observations

Spectroscopic data on HD 93403 were obtained during several runs spread over a bit more than two years (from February 1998 till May 2000). The data set consists of observations gathered with various instruments at the European Southern Observatory (ESO) at La Silla and at the Cerro Tololo Inter-American Observatory (CTIO). Table 1 presents the journal of the observations.

Twenty high resolution spectra of the He I λ 4471 line were obtained with ESO's 1.4 m Coudé Auxiliary Telescope (CAT) at La Silla, using the Coudé Echelle Spectrometer (CES) equipped with the Long Camera (LC, before March 1998) or the Very Long Camera (VLC, after March 1998). The detector used was ESO CCD#38, a Loral 2688×512 pixel CCD with a pixel size of $15\ \mu$m$\times 15\ \mu$m. The slit width was chosen to achieve a nominal resolution of 70000–80000. The effective resolving power as derived from the FWHM of the lines of the ThAr calibration exposures is 60000–75000. Typical exposure times were of the

Send offprint requests to: G. Rauw (rauw@astro.ulg.ac.be)

⋆ Based on observations collected at the European Southern Observatory (La Silla, Chile) and the Cerro Tololo Inter-American Observatory (CTIO).

⋆⋆ Postdoctoral Researcher FNRS (Belgium)

⋆⋆⋆ Research Associate FNRS (Belgium)

† Visiting Astronomer, CTIO, National Optical Astronomy Observatories (NOAO). NOAO is operated by the Association of Universities for Research in Astronomy, Inc. under contract with the National Science Foundation.

order of 45 minutes and the average S/N ratio is above 100. The wavelength domain is centered on the He I λ 4471 line and is ~ 40 Å and ~ 20 Å wide for spectra taken with the LC and the VLC respectively.

During three observing runs in April – May 1999, end of May 1999 and early May 2000, a set of echelle spectra was gathered with the Fiber-fed Extended Range Optical Spectrograph (FEROS, Kaufer et al. 1999) attached to the ESO 1.52 m telescope at La Silla. Thirty seven orders corresponding to a wavelength domain from 3650 to 9200 Å were observed. Typical exposure times were of the order of 10–15 minutes and the average S/N ratio is about 65, 150 and 110 at 4050, 6000 and 7500 Å respectively. The spectral resolving power of the FEROS instrument is 48000. The detector was an EEV CCD with 2048×4096 pixels of $15\,\mu$m$\times 15\,\mu$m. For a detailed description of the spectrograph, we refer the reader to the paper of Kaufer et al. (1999).

Finally, another set of echelle spectra over the range 3850 to 5790 Å was obtained with the Bench-Mounted Echelle Spectrograph (BME) attached to the 1.5 m CTIO Ritchey-Chretien Telescope, during a 5 night run in June 1999. Forty nine orders were observed using the KPGL2 316 lines mm^{-1} grating as a cross-disperser. The detector was a Tek 2048 CCD with 24 μm pixels. The slit width was set to 70μm corresponding to a resolving power of 45000. Exposure times ranged from one hour to two hours depending on the weather conditions and the S/N ratio in the continuum is about 80.

2.2. Data reduction

The CAT observations were reduced in a standard way using the MIDAS package provided by ESO. The spectra of HD 93403 were rectified by means of an instrumental response curve built from observations of a metal-poor 'reference' star with weak narrow absorption lines. When such a reference spectrum was not available, we performed the normalization by fitting a polynomial to the continuum.

We used the FEROS context working under the MIDAS environment to reduce the FEROS echelle spectra. We slightly adapted the MIDAS routines kindly provided by Dr. O. Stahl in order to match the current configuration of the FEROS instrumentation. The reduction was performed using both *standard* and *optimum* options. It turned out that the *standard* option yields slightly better results, probably due to the important number of bad columns on the CCD. Most of the unavoidable strong fringes that affect the red part of the spectrum (above 6600 Å) are simply corrected by flat-fielding. There are however a few residual fringes near 6670, 7140 and 7385 Å. In order to achieve a good S/N ratio around the order connections in the blue, the orders were merged by averaging the overlapping areas over a 30 Å range. Due to particularly precarious weather conditions, the FEROS observations of the end of May 1999 run result from the addition of several spectra taken during the same night. Finally, the FEROS spectra were normalized over a range of a few hundred Å at once by fitting a polynomial of degree 4 or 5 to the continuum.

Table 1. Journal of the observations of the He I λ 4471 absorption line. The first column gives the Heliocentric Julian Date (HJD) in the format HJD–2450000. The next two columns give the measured radial velocity, expressed in km s^{-1}, for the primary and secondary respectively. For those spectra where we were not able to separate the blended lines, only the radial velocity of the blend is listed. The fourth column reports the method used to measure the RVs: 1=one gaussian fit, 2=two gaussian fit, 3=cross-correlation like method. The fifth column identifies the instrumentation. The last column provides the orbital phases of the observations relative to the time of periastron passage ($T_0 = 2451355.643$) as derived from our new common orbital solution given in Table 5.

Date	$v_{r,1}$	$v_{r,2}$	Method	Intrument.	ϕ
857.868	69.2	-146.0	2	CES+LC	0.019
859.644	-18.2		1	CES+LC	0.137
860.633	-19.6		1	CES+LC	0.203
861.626	-57.8	87.0	2	CES+LC	0.268
862.625	-62.2	104.2	2	CES+LC	0.335
864.607	-70.2	106.2	2	CES+LC	0.466
925.649	-70.3	91.2	2	CES+VLC	0.510
926.605	-52.0	82.8	2	CES+VLC	0.574
928.509	-18.5		1	CES+VLC	0.700
931.486	70.8	-146.4	2	CES+VLC	0.897
932.472	81.1	-171.5	2	CES+VLC	0.962
933.487	59.4	-137.3	2	CES+VLC	0.030
934.484	-23.4		1	CES+VLC	0.096
936.527	-66.4	60.4	3	CES+VLC	0.231
939.468	-70.3	99.7	2	CES+VLC	0.426
995.580	-16.0		1	CES+VLC	0.144
996.537	-50.8	36.4	3	CES+VLC	0.207
998.543	-80.6	96.8	2	CES+VLC	0.340
999.543	-74.6	101.3	2	CES+VLC	0.406
1000.503	-78.4	97.9	2	CES+VLC	0.470
1299.704	-64.7	93.3	2	FEROS	0.294
1300.712	-75.2	97.5	2	FEROS	0.360
1301.692	-75.7	102.2	2	FEROS	0.425
1302.697	-72.8	97.7	2	FEROS	0.492
1304.710	-52.7	49.3	3	FEROS	0.625
1322.507	9.7	-83.5	3	FEROS	0.804
1323.669	66.2	-140.8	2	FEROS	0.882
1327.501	-26.5	-9.1	3	FEROS	0.135
1328.530	-24.6		1	BME	0.206
1329.471	-53.2	55.5	3	BME	0.266
1330.497	-82.0	87.3	2	BME	0.334
1331.575	-82.1	96.6	2	BME	0.405
1332.585	-82.2	89.2	2	BME	0.472
1669.664	27.9	-76.9	3	FEROS	0.806
1670.655	49.9	-130.1	2	FEROS	0.871
1671.657	75.9	-169.3	2	FEROS	0.938
1672.640	78.5	-165.7	2	FEROS	0.003
1673.624	42.2	-121.1	3	FEROS	0.068

The BME data were reduced using the IRAF[1] package and following the recommendations of the BME User's Manual. The pixel to pixel variations were removed using flat field exposures

[1] IRAF is distributed by the National Optical Astronomy Observatories.

Table 2. Radial velocities of several lines measured on FEROS and BME spectra. The notations are identical to those used in Table 1.

Date	O III λ 5592			C IV λ 5801			C IV λ 5812			He I λ 5876		
	$v_{r,1}$	$v_{r,2}$	Method	$v_{r,1}$	$v_{r,2}$	Method	$v_{r,1}$	$v_{r,2}$	Method	$v_{r,1}$	$v_{r,2}$	Method
1299.704	−59.8	90	2	−55.0	90.8	2	−65.0	93.8	2	−63.1	81.4	2
1300.712	−74.1	106.7	2	−71.0	108.9	2	−74.2	105.9	2	−68.9	96.4	2
1301.692	−70.3	116.7	2	−59.7	115.3	2	−70.3	104.0	2	−70.2	108.8	2
1302.697	−71.6	99.0	2	−63.7	103.0	2	−73.1	99.1	2	−68.1	99.2	2
1304.710	−52.8	65.0	3	−20.7		1	−46.3	60.7	3	−43.2	46.2	3
1322.507	42.1	−74.9	3	31.4	−87.7	3	24.9	−91.7	3	19.5	−71.6	3
1323.669	79.0	−134.6	2	68.8	−130.3	2	64.7	−134.0	2	69.3	−132.7	2
1327.501	−21.0	18.1	3	−0.8		1	−15.3	10.7	3	−15.7	−5.8	3
1328.530	−15.8		1									
1329.471	−47.9	64.7	2									
1330.497	−86.2	92.0	2									
1331.575	−72.0	116.3	2									
1332.585	−77.0	113.4	2									
1669.664	25.3	−64.1	3	41.3	−66.5	3	4.3		1	22.6	−64.3	3
1670.655	60.2	−128.0	2	70.8	−136.2	2	55.6	−126.0	2	57.6	−120.0	2
1671.657	92.7	−172.0	2	96.5	−185.1	2	90.8	−158.1	2	84.0	−166.8	2
1672.640	93.1	−169.3	2	97.1	−186.1	2	94.9	−154.8	2	84.8	−160.9	2
1673.624	60.6	−97.1	2	70.7	−89.7	3	59.7	−103.4	2	47.2	−102.1	2

taken with a very bright light source and a diffusing screen placed inside the spectrograph (so-called *milky flats*). A first rectifying of the extracted echelle orders was carried out with the projector flat exposures. Finally, the spectra were normalized by fitting a low-order polynomial to the continuum. As the exposure time of individual spectra was limited to one hour, we added up the spectra taken during the same night in order to reach a higher S/N ratio. For those nights where we have added several exposures, the dates listed in Table 1 and Table 2 correspond to the mean time.

2.3. Radial velocity measurements

The radial velocities (RVs) were measured by fitting two gaussians to the absorption lines whenever the separation was sufficient to do so. When this was not the case, we used a cross-correlation like technique in an attempt to deblend the lines of the two components of the system. To do so, we built a template of the individual absorption lines derived from the fit to the spectra when the separation is maximum and we shifted both fake lines until we achieved an acceptable fit to the blend. Near the conjunctions, this technique yields usually two possible solutions and we selected the most likely one by comparison with the spectra obtained at adjacent orbital phases. Probably as a result of some slight line profile variability, we notice that the templates do not perfectly match the line profiles near conjunction. This leads to intrinsically larger error bars on the RVs measured near conjunction and these RVs were thus assigned a lower weight in the orbital solution (see Sect. 3). The measured RVs and the method used to deblend the lines are reported in Tables 1 and 2. The effective rest wavelengths used in the RV computations are given in column 2 of Table 3 and were adopted from Underhill (1995) except for the He I λ 4471 line where we used the result of Conti et al. (1977).

Table 3. Adopted effective wavelengths, average equivalent width ratios (primary/secondary) measured on our spectra and corresponding luminosity ratios corrected for the different spectral types (see text).

Spectral line	λ_0 (Å)	EW ratio	$L^{\rm prim}/L^{\rm sec}$
He I λ 4471	4471.512	2.15	4.6
O III λ 5592	5592.370	2.64	4.0
C IV λ 5801	5801.330	3.83	4.0
C IV λ 5812	5811.980	4.81	5.0
He I λ 5876	5875.620		

2.4. Spectral features

The FEROS instrument offers the opportunity to investigate nearly the entire optical spectrum of HD 93403. Selected spectral ranges are shown in Fig. 1. The main spectral lines are indicated. The most outstanding spectral features of HD 93403 are described below.

- The He II λ 4686 line consists of a mixture of absorption and emission components. Its profile presents obvious but complex night-to-night variations. A preliminary analysis shows that the wavelength variations of the absorption component follow the secondary RV curve. The emission component appears quite broad and we suspect rather fast profile variations. Whether this is the signature of a wind interaction process is unclear. Additional high quality data are required to clarify the nature of these variations and we have to defer a discussion of the He II λ 4686 line profile variations to a forthcoming paper.
- Both the primary and the secondary spectra show the C III λ 5696 line in emission. We have measured the phase-dependent RVs of both components and the results are in fair agreement with the orbital solutions derived from the absorption lines. This result is in line with a photospheric

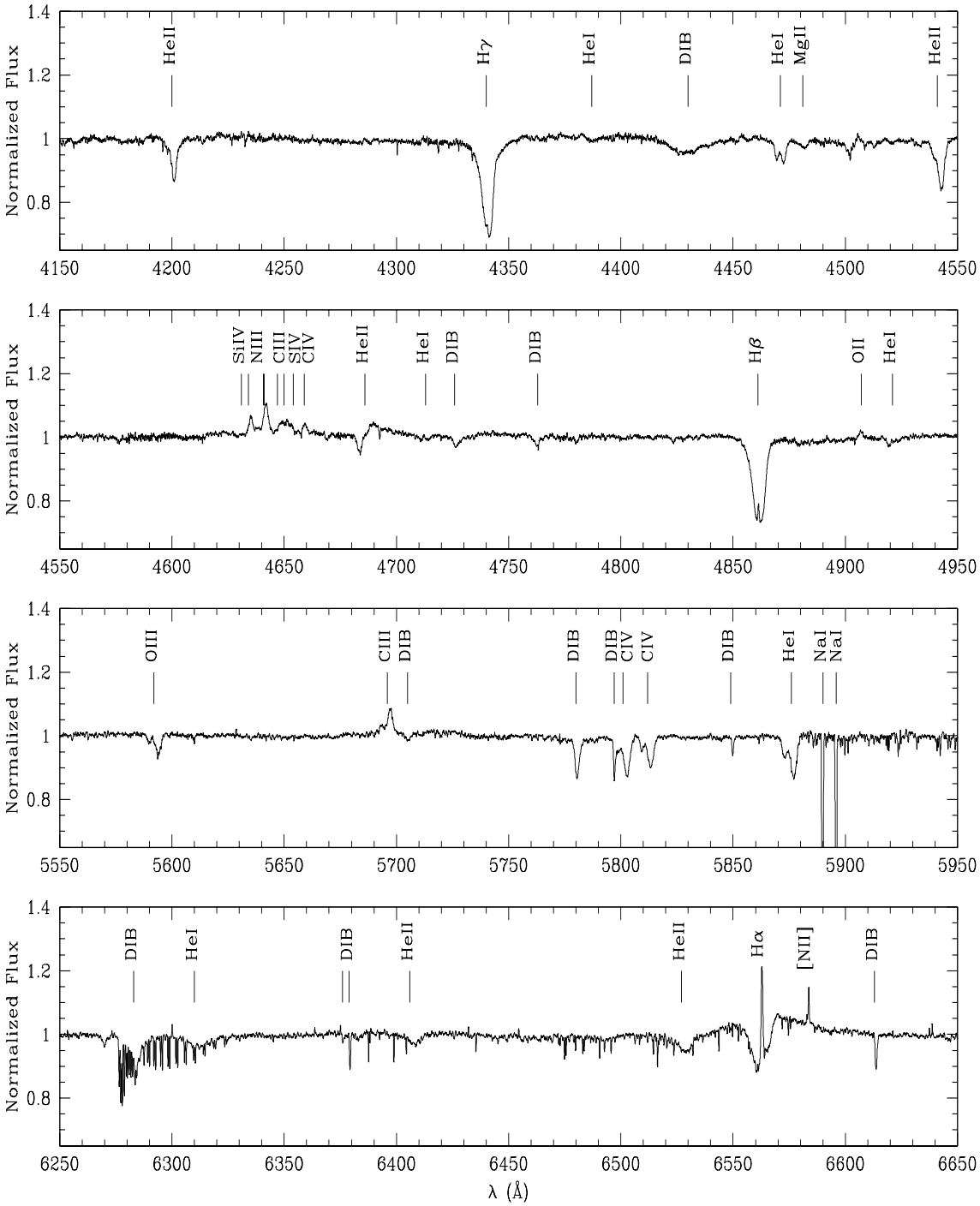

Fig. 1. FEROS spectrum of HD 93403 as observed on HJD 2451323.669.

origin of the C III λ 5696 emission line in the spectra of O stars as suggested by Nussbaumer (1971) and Cardona-Núñez (1978) and lends further support to our orbital solution.

– The Hα line profile is rather complex. It is composed of an absorption component superimposed on a broader emission. Thaller (1997) claimed that the Hα profile was variable. However, our data reveal only subtle night-to-night variability and the line profile analysis is further complicated by a rather prominent nebular emission line.

– Finally, we investigate the interstellar Ca II and Na I lines (Fig. 2). Though Walborn & Hesser (1975) report single Ca II H and K lines, we could detect an additional blueshifted fainter component around $-23\,\mathrm{km\,s^{-1}}$. The profile of the stronger Ca II component is most probably formed by two heavily blended lines. The Na I lines also show a fainter blueshifted component, with a velocity similar to that of the

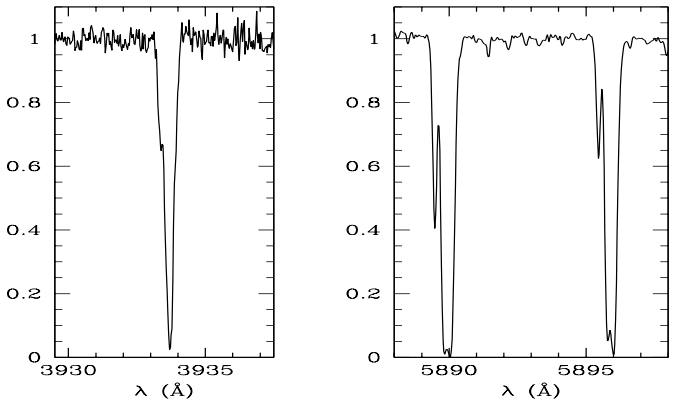

Fig. 2. Interstellar Ca II K and Na I D1 and D2 profiles in the spectrum of HD 93403.

Table 4. Mean RVs and EWs of Ca II and Na I interstellar lines. The quoted uncertainties correspond to the standard deviation of our measurements.

Spectral line	RV (km s^{-1})			EW (mÅ)		
Ca II K λ 3933	-24.0	$\pm$	0.8	50	$\pm$	6
	2.9	$\pm$	0.6	382	$\pm$	9
Ca II H λ 3968	-22.0	$\pm$	1.1	31	$\pm$	6
	2.9	$\pm$	0.2	196	$\pm$	12
Na I D2 λ 5890	-23.6	$\pm$	0.2	108	$\pm$	2
	-7.6	$\pm$	0.3	209	$\pm$	11
	6.0	$\pm$	0.3	337	$\pm$	12
Na I D1 λ 5896	-23.2	$\pm$	0.2	66	$\pm$	1
	-7.6	$\pm$	0.2	166	$\pm$	6
	4.9	$\pm$	0.2	320	$\pm$	8

Ca II one. The strongest Na I component clearly reveals a double peaked profile. We have measured the RVs and the equivalent widths on the FEROS spectra. Our results are listed in Table 4. They are in qualitative agreement with previous measurements (Walborn & Hesser 1975, Walborn 1982). We should emphasize here the good night-to-night stability of the FEROS spectrograph as the dispersion of the measured radial velocities of the interstellar lines is rather low.

3. Orbital Solution

The orbital solution was computed using a modified version of the Wolfe, Horak & Storer algorithm (Wolfe et al. 1967, WHS hereafter). Knowing the observation dates, the RVs and the period, the original WHS method allows to compute the orbital solution associated to one component of the system at once, which is of course sufficient for an SB1 system. Applying this method to SB2 systems leads however to a priori independent orbital elements for both components of the system, as only the RVs associated to one star are taken into account. For instance, this problem typically leads to two distinct values of the eccentricity and of the time of periastron passage. We have therefore modified the WHS method to circumvent this problem and to take into account the primary and secondary RVs simultaneously.

Our approach is based on the following straightforward relation between the RVs of the two components of the binary system:

$$v_2(\phi) = c\, v_1(\phi) + b \qquad (1)$$

with $c = -K_2/K_1 = -m_1/m_2$ and $b = \gamma_1\, K_2/K_1 + \gamma_2$.

m_i, $v_i(\phi)$ and K_i are respectively the mass, the radial velocity at orbital phase ϕ and the amplitude of the radial velocity curve of the i-th component of the system. γ_i is the *apparent* systemic velocity as deduced from the spectrum of the i-th component. Since it is not unusual to find quite different apparent systemic velocities for the components of an evolved early-type binary (e.g. Rauw et al. 1999), we will consider a priori distinct values of γ_i for both stars.

We first fit a straight line to the data in the $(v_{r,1}, v_{r,2})$ plane. This is done using an orthogonal regression as both coordinates are affected by errors of the same order of magnitude. The best fit relation immediately provides us with the mass ratio of the system and it further allows us to express the RVs associated with one star of the system as a function of those of its companion. We are then able to convert all the RV data to equivalent RVs of one component and thus to run the WHS code taking into account the complete data set. We adopt a unity weight for the RVs measured by fitting two well separated gaussians, while we set the weight of the RVs near conjunction to a value two to ten times lower, according to the quality of the cross-correlation fit. Those lines that we were not able to deblend were attributed a zero weight.

We first adopted a period of 15.093 days, as derived by TE. Table 5 gives both individual and joint orbital solutions as computed in the way described just here above. We chose the primary to be the most massive and most luminous star of the system. Fig. 3 displays the RV curves of HD 93403.

4. Discussion

Our new orbital solution differs significantly from the one of Thackeray & Emerson (1969), especially with respect to the value of the eccentricity which we find to be about half their value. We re-computed the orbital elements using TE's data and we recovered their published values. We believe that the discrepancy between their solution and ours arises from the fact that they were unable to separate both components on most of their spectra. This could lead to underestimate the primary RVs except near phases of maximum RV separation. As a result the RV curve displays an apparently narrower peak, leading to the determination of a higher eccentricity. Another discrepancy concerns the difference in the longitude of periastron ω of about $34°$. Interpreted in terms of an apsidal motion, it would correspond to a rate of apsidal motion of about $1°$ per year, which is an unexpectedly high value for such a system. Therefore, it seems likely that at least part of this difference is an artefact due to the above mentioned bias in TE's radial velocities.

Table 5. Computed orbital solution for HD 93403 using the RVs of the He I λ 4471 absorption lines. T_0 is the time of the periastron passage.

	Common solution			Individual Solutions					
				Primary			Secondary		
P(days)	15.093 (fixed)			fixed			fixed		
e	0.234	$\pm$	0.021	0.237	$\pm$	0.031	0.229	$\pm$	0.021
$\omega(^o)$	22.5	$\pm$	4.4	22.2	$\pm$	6.4	202.9	$\pm$	4.4
T_0(HJD-2450000)	1355.643	$\pm$	0.158	1355.629	$\pm$	0.231	1355.660	$\pm$	0.162
γ_1 (km s^{-1})	-14.8	$\pm$	1.2	-15.0	$\pm$	1.8			
K_1 (km s^{-1})	79.3	$\pm$	1.1	79.4	$\pm$	1.6			
$a_1 \sin i$ (R$_\odot$)	22.9	$\pm$	0.3	22.9	$\pm$	0.5			
γ_2 (km s^{-1})	-5.4	$\pm$	4.5				-5.8	$\pm$	2.1
K_2 (km s^{-1})	139.0	$\pm$	4.9				138.7	$\pm$	1.8
$a_2 \sin i$ (R$_\odot$)	40.3	$\pm$	1.7				40.3	$\pm$	0.6
$q(m_1/m_2)$	1.753	$\pm$	0.057						
$m_1 \sin^3 i$ (M$_\odot$)	9.52	$\pm$	0.82						
$m_2 \sin^3 i$ (M$_\odot$)	5.43	$\pm$	0.33						
rms$(O-C)$ (km s^{-1})	5.0			5.8			6.7		

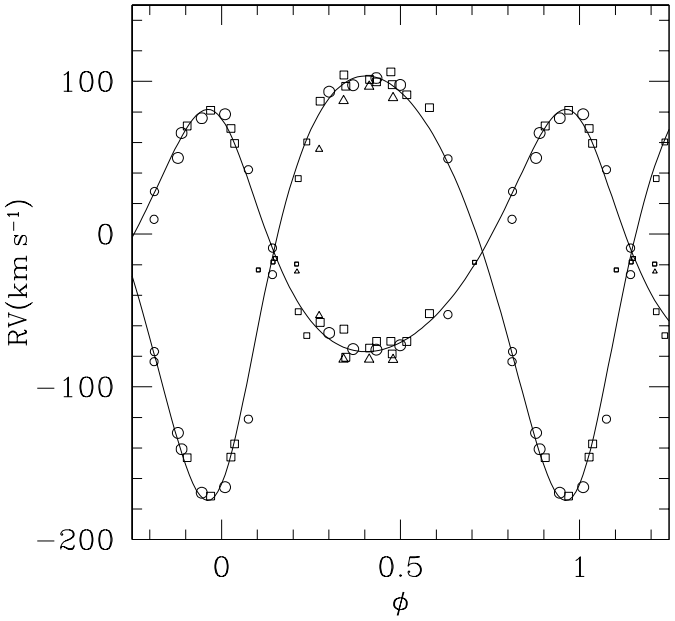

Fig. 3. Radial velocity curve of the HD 93403 binary system. Different symbols refer to different instruments: triangle=BME, square=CES, circle=FEROS. Different sizes indicate different weights assigned to the data points in the orbital solution.

We next turn to the problem of the orbital period of the system. One point was to look for any significant change over the last thirty years. Another was to try to improve TE's value. To do so, we used the method of Lafler & Kinman (1965) and a Fourier analysis to derive the orbital period from our RV data. Both techniques yield values that lie within 0.02 days of TE's value, which is well below the estimated uncertainty (the FWHM of the peak in the power spectrum corresponds to 0.25 days) of our period determination. We then allowed differential corrections for the period while running our orbital solution code (see WHS, 1967). The value found in this way is 15.096 ± 0.002 days, which again is in fair agreement with TE's value. We conclude therefore that there is no evidence for a variation of the period and, owing to the above mentioned bias, we think wise to adopt TE's value of 15.093 days.

In addition to the He I λ 4471 line, four other absorption lines (namely O III λ 5592, C IV λ 5801, C IV λ 5812 and He I λ 5876) reveal the signature of both components except near conjunction. We used the mean RVs associated to these lines and the He I λ 4471 line, measured on FEROS spectra, to derive another orbital solution. The resulting parameters overlap within the errors with those of Table 5.

Four FEROS spectra could be obtained when the separation between the components' lines reached its maximum (around phases 0.9 to 0.1; see Fig. 1). Six more lines could be deblended on these spectra: He I λ 4026, He II λ 4200, Mg II λ 4481, He II λ 4541, He II λ 5412 and He I λ 7065. Following Conti (1973), we then use the ratio of the equivalent widths of the He I λ 4471 and He II λ 4541 lines ($\log W(\frac{\lambda\,4471}{\lambda\,4541})$, see his Table 1) for the primary and the secondary respectively, in order to derive a spectral classification for the two components. We get average values of $\log W^{\rm prim} = -0.40 \pm 0.04$ and $\log W^{\rm sec} = -0.10 \pm 0.03$. According to this criterion, HD 93403 is an O5.5 + O7 system. It is worth noting here that this result is in very good agreement with the spectral types proposed by TE 30 years ago, and with the ones derived by Penny (1997) from UV data.

We can derive a rough estimate of the luminosity ratio between the components of HD 93403 by comparing the intensities of their absorption lines. Using a cross-correlation technique to analyse IUE spectra, Howarth et al. (1997) found a difference in magnitude between the two stars of $\Delta\, m' = 1.1$. This result did however not include a correction for the difference in spectral type between the components of HD 93403 and corresponds to the only two IUE spectra obtained near periastron and which showed well resolved cross-correlation peaks. The mean intensity ratios measured on our observations are listed in Table 3. In order to derive the luminosity ratio, the measured intensity

ratios must be corrected for the spectral type difference of the components. From the results of Conti & Alschuler (1971), we expect an average ratio of ~ 0.47 between the equivalent width of the He I λ 4471 absorption lines of a typical single O5.5 star and a single O7 star. Therefore, the observed line intensity ratio corresponds to a corrected luminosity ratio of ~ 4.6. The trend of the O III λ 5592 and C IV $\lambda\lambda$ 5801, 5812 line intensities with spectral type is less clear cut (Conti 1974, Walborn 1980). We have nevertheless used the equivalent widths tabulated by Conti (1974) to estimate average equivalent width ratios for single stars. The corrected luminosity ratios (Table 3) confirm the result obtained for the He I λ 4471 line. We caution however that the strength of the C IV lines in the spectrum of the secondary star shows a phase dependence and the equivalent widths increase by about a factor of two in the phase interval 0.9–0.1. Whether this phenomenon is related to the so-called 'Struve-Sahade' effect (Stickland 1997) is not clear. These EW variations are much less pronounced for the He I λ 4471 and O III λ 5592 lines. In the following, we adopt the mean value derived from these two lines, yielding a luminosity ratio of 4.3 between the primary and the secondary. It is worth noting that this luminosity ratio is larger than the value expected (~ 1.7, Howarth & Prinja 1989) if both stars were of giant luminosity class as suggested by Penny (1997). Therefore it seems more likely that the two components have different luminosity classes. The fact that He II λ 4686 is found in absorption in the spectrum of the secondary star while the line is not seen in absorption in the primary's spectrum lends further support to this conclusion.

Assuming that the primary is a giant and the secondary a main sequence star and adopting the effective temperature calibration of Chlebowski & Garmany (1991), the spectral types derived above yield $T_{\rm eff} = 41300 \pm 1100$ K and $T_{\rm eff} = 40100 \pm 1100$ K for the primary and the secondary respectively. Given the good agreement between the spectral types derived by different investigators, we assume a typical uncertainty of half a spectral subtype.

Kaltcheva & Georgiev (1993) report $V = 7.30$ and $E(B-V) = 0.49$ for HD 93403. Assuming $A_V = 3.2 \times E(B-V)$ and adopting an average distance modulus of 12.55 to the Tr 16 cluster (Massey & Johnson 1993), we obtain $\log(L_{\rm bol}^{\rm prim}/L_\odot) = 6.08 \pm 0.2$ and $\log(L_{\rm bol}^{\rm sec}/L_\odot) = 5.41 \pm 0.2$ for the primary and secondary respectively. The locations of the components of HD 93403 are plotted in a H-R diagram in Fig. 4 together with the theoretical models of Schaller et al. (1992). The primary star is the most evolved component of the system, whereas the secondary lies still close to the ZAMS. A crude interpolation between the evolutionary tracks of Schaller et al. (1992) yields $M_1 = 75.5^{+8.2}_{-16.4}\,{\rm M}_\odot$ and $M_2 = 37.3^{+7.2}_{-4.2}\,{\rm M}_\odot$. The theoretical mass ratio of $2.02^{+.51}_{-.69}$ is larger than the observed value (1.753 ± 0.057) but we emphasize that this theoretical mass ratio is rather sensitive to the adopted distance of HD 93403 and to the luminosity ratio between the two stars.

If we repeat the above procedure assuming this time that the primary is a supergiant and the secondary a giant star, we obtain $T_{\rm eff} = 39300 \pm 1100$ K, $\log(L_{\rm bol}^{\rm prim}/L_\odot) = 6.02 \pm 0.2$ and $T_{\rm eff} = 38100 \pm 1100$ K, $\log(L_{\rm bol}^{\rm sec}/L_\odot) = 5.35 \pm 0.2$ for the primary and the secondary respectively. This time, comparison with the models of Schaller et al. (1992) yields masses of $M_1 = 68.5^{+12.3}_{-14.6}\,{\rm M}_\odot$ and $M_2 = 34.8^{+4.7}_{-4.4}\,{\rm M}_\odot$. Our conclusion about the theoretical mass ratio ($1.97^{+.69}_{-.61}$) remains valid although we find a slightly better agreement with the observed value. Finally, if we assume that the primary is a supergiant and the secondary is a main sequence object, we get a theoretical mass ratio of $1.84^{+.60}_{-.63}$.

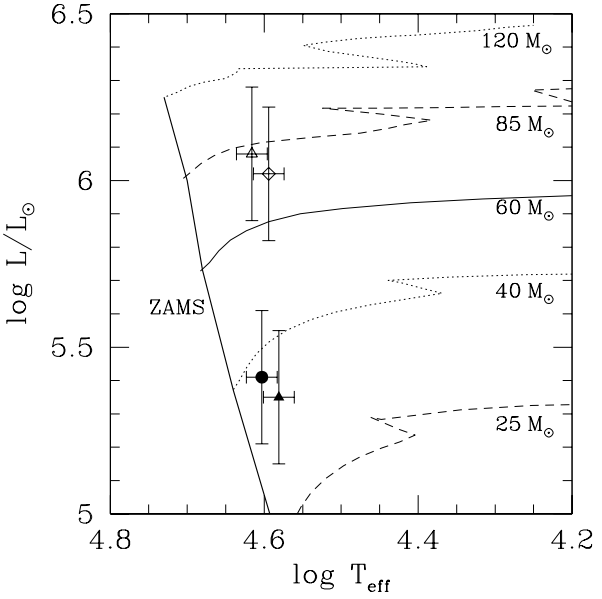

Fig. 4. Hertzsprung-Russell diagram of the HD 93403 system. The open and filled symbols stand for the primary and secondary respectively. Different symbols stand for different assumptions on the luminosity class (and hence the bolometric correction): circles, triangles and diamonds correspond to luminosity classes V, III and I respectively. The evolutionary tracks are from Schaller et al. (1992) for Z=0.020 and adopting 'standard' mass loss rates.

Comparing our results with the typical parameters of O stars listed by Howarth & Prinja (1989), we find the best overall agreement if we assume that the primary is an O5.5 I supergiant and the secondary an O7 V main sequence star.

We can use the above results to discuss some constraints on the geometry of the system adopting typical parameters for O5.5 I and O7 V stars (see e.g. Howarth and Prinja 1989). From the typical radii ($R_{\rm O5.5\,I} \simeq 24\,{\rm R}_\odot$; $R_{\rm O7\,V} \simeq 10\,{\rm R}_\odot$) and assuming that HD 93403 is a non-eclipsing system, we can set an upper limit on the orbital inclination i of 58.2°. Using the minimum masses corresponding to our orbital solution (Table 5) this upper limit on i corresponds to lower limits of 15.5 $\rm M_\odot$ and 8.8 $\rm M_\odot$ for the mass of the primary and secondary respectively. If we further impose that the primary's mass should be less than 120 $\rm M_\odot$, which seems a reasonable limit, we get $i \geq 25°$.

Adopting a mass of 68.5 $\rm M_\odot$ for the O5.5 I primary, we get a first crude estimate for the orbital inclination: $i \approx 31.2°$. Applying the same argument ($M_{\rm O7\,V} \simeq 37.3\,{\rm M}_\odot$) to the secondary yields an inclination of 31.7°, in excellent agreement with the value for the primary star. Though this is a very crude method

to estimate i, it will certainly be useful for the interpretation of the forthcoming X-ray data.

Although the Roche equipotential model is certainly not well justified for a binary system with an eccentricity of 0.234, we can derive first order constraints on the configuration of the binary from the radii of the 'instantaneous' Roche lobe (R_{RL}) around periastron passage. To this end, we adapt Eggleton's formula (Eggleton 1983):

$$\frac{R_{RL}}{a} = (1-e)\,\frac{0.49\,q^{2/3}}{0.6\,q^{2/3}+\ln(1+q^{1/3})} \qquad (2)$$

where a is the total semi-major axis of the binary and q is the mass ratio. Using $a \sin i = 63.2\,\mathrm{R}_\odot$, we get the minimum values of:

$$\begin{cases} R_{RL,1} \sin i = 20.7\,\mathrm{R}_\odot \\ R_{RL,2} \sin i = 16.0\,\mathrm{R}_\odot \end{cases}$$

As the 'typical' radii for O5.5 I and O7 V stars are $24\,\mathrm{R}_\odot$ and $10\,\mathrm{R}_\odot$ respectively, the stars in HD 93403 are unlikely to undergo 'Roche lobe overflow' near periastron. Assuming an inclination of $i \approx 32°$, the primary and secondary should fill respectively about 23% and 4% of their critical volume at periastron passage.

5. Conclusion

We have presented a spectroscopic analysis of the early-type binary HD 93403. As this system is scheduled for observations with ESA's recently launched XMM satellite, one aim of this study was to derive accurate orbital parameters. Using high resolution observations, we have been able to separate the primary and secondary component of the binary. For the first time, an orbital solution for both stars of the system has been computed. This new solution differs significantly from the previous one obtained by TE. This may result from a bias in TE's data due to the fact that they did not separate the primary and secondary spectra.

Based on the He I λ 4471 and He II λ 4541 equivalent width ratio, we derive an O5.5 and O7 spectral type for the primary and secondary respectively. This is in fair agreement with previous spectral-type determinations including the results of the tomographic analysis of IUE data by Penny (1997). Due to the presence of He II λ 4686 in absorption in the secondary spectrum and to the relatively high spectroscopic luminosity ratio between the primary and secondary, we also suggest that the secondary could be a main sequence star and would therefore be the less evolved component of the system whereas the primary is probably a more evolved supergiant.

Using typical parameters for O-type stars, we derived qualitative constraints on the inclination of the system: $25° < i < 58°$ with a 'reasonable' value around $31°$ to $32°$. We further underline that HD 93403 should not be currently undergoing a 'Roche lobe overflow' process. The low orbital inclination makes this system a highly interesting target for studying the effects of a non zero eccentricity on the intrinsic X-ray emission generated in a colliding wind process. In fact, given this low inclination, we expect little variability of the circumstellar column density towards the shock cone as a function of orbital phase. Since the column density remains probably roughly constant, any orbital variability of the X-ray emission would most probably be due to the changing separation between the two stars (Pittard & Stevens 1997).

Finally we note the complex line profile variability of the He II λ 4686 line. Unfortunately our phase coverage of this spectral region is not sufficient to investigate the phase dependence of this variability. More high resolution and high S/N ratio spectra are needed to investigate possible fast line profile variability. In light of a possible wind interaction between the components of HD 93403, the comparison of the line profile variability of He II λ4686 with the forthcoming X-ray data could be of crucial importance to constrain the nature of the interaction process.

Acknowledgements. We wish to thank Dr. O. Stahl for his efficient help in adapting the FEROS reduction package to our data. We are grateful to Y. Nazé and Dr. J. Manfroid for their help in the reduction of the BME data and to A. Kransvelt for his assistance during the commissioning of the VLC instrument. We are greatly indebted to the Fonds National de la Recherche Scientifique (Belgium) for multiple supports. This research is also supported in part by contract P4/05 "Pôle d'Attraction Interuniversitaire" (SSTC-Belgium). Partial support through the PRODEX XMM-OM Project is also gratefully acknowledged. The SIMBAD database has been consulted for the bibliography.

References

Cardona-Núñez O., 1978, PhD Thesis, University of Colorado, Boulder
Chlebowski T., Garmany C.D., 1991, ApJ 368, 241
Conti P.S., 1973, ApJ 179, 181
Conti P.S., 1974, ApJ 187, 539
Conti P.S., Alschuler W.R., 1971, ApJ 170, 325
Conti P.S., Frost S.A., 1977, ApJ 212, 728
Conti P.S., Leep E.M., Lorre J.J., 1977, ApJ 214, 759
Eggleton P.P., 1983, ApJ 268, 368
Feast M.W., Thackeray A.D., Wesselink A.J., 1955, Mem. R. Astr. Soc. 67, 51
Howarth I.D., Prinja R.K., 1989, ApJS 69, 527
Howarth I.D., Siebert K.W., Hussain G.A.J., Prinja R.K., 1997, MNRAS 284, 265
Kaltcheva N.T., Georgiev L.N., 1993, MNRAS 261, 847
Kaufer A., Stahl O., Tubbesing S. et al., 1999, The Messenger 95, 8
Lafler J., Kinman T.D., 1965, ApJS 11, 216
Massey P., Johnson J., 1993, AJ 105, 980
Nussbaumer H., 1971, ApJ 170, 93
Penny L.R., 1997, PASP 109, 848
Pittard J.M., Stevens I.R., 1997, MNRAS 292, 298
Rauw G., Vreux J.-M., Bohannan B., 1999, ApJ 517, 416
Schaller G., Schaerer D., Meynet G., Maeder A., 1992, A&AS 96, 269
Seward F.D., Forman W.R., Giacconi R. et al., 1979, ApJ 234, L55
Stickland D.J., 1997, The Observatory 117, 37
Thackeray A.D., Emerson B., 1969, MNRAS 142, 429
Thaller M.L., 1997, ApJ 487, 380
Underhill A.B., 1995, ApJS 100, 433
Walborn N.R., 1972, AJ 77, 312
Walborn N.R., 1980, ApJS 44, 535
Walborn N.R., 1982, ApJS 48, 145
Walborn N.R., Hesser J.E., 1975, ApJ 199, 535
Wolfe R.H. Jr., Horak H.G., Storer N.W., 1967. In: Modern Astrophysics, Hack M. (ed.), Gordon & Breach, New York, 251